

The quantum $\text{AdS}_5 \times \text{S}^5$ superstring at finite coupling

R. W. McKeown and R. Roiban

*Department of Physics, The Pennsylvania State University,
University Park, PA 16802, USA*

Abstract

The integrability of string theory in $\text{AdS}_5 \times \text{S}^5$ and of the dilatation operator of $\mathcal{N} = 4$ super-Yang-Mills theory has been used to propose an exact solution to the spectral problem in these theories. Weak coupling perturbation theory both in gauge theory and on the worldsheet has been extensively used to verify this solution.

We discuss worldsheet methods for finding the spectrum of the $\text{AdS}_5 \times \text{S}^5$ superstring at finite values of the coupling constant and illustrate them by recovering, within numerical errors, the predictions of the BES equation for the universal scaling function. This is the first finite-coupling calculation in this theory which uses field theory methods.

Contents

1	Introduction	3
2	A numerical approach to the Green-Schwarz string	5
2.1	A first pass at a discrete Green-Schwarz action in $\text{AdS}_5 \times \text{S}^5$	5
2.2	Various approaches to energy calculations	8
2.2.1	A conformal gauge approach	8
2.2.2	Operator dimensions from the boundary two-point functions	10
2.2.3	Target space energy from a partition function	12
3	An example: the universal scaling function at finite coupling	13
3.1	The null cusp fluctuation action, discretization, and some numerical details . .	14
3.2	The simulation, data analysis and results	16
4	Summary and further comments	20
A	Simulating the lattice: Algorithms	22
A.1	The Rational Hybrid Monte Carlo algorithm	22
A.2	Monte Carlo methods	22
A.3	The HMC algorithm	23
A.4	The fermion contribution to bosonic RHMC forces	24
A.5	A summary of sources of errors	25
B	9-point stencil	26
B.1	ρ matrices	27
C	Fermions	27

1 Introduction

Superstring theory in $\text{AdS}_5 \times \text{S}^5$ is described by a complicated interacting two-dimensional field theory of Green-Schwarz type; solving it exactly appears to be a difficult problem. From a conformal field theory perspective one is interested in finding vertex operators labeled by $\text{PSU}(2, 2|4)$ quantum numbers $\hat{C} = (E; S_1, S_2; J_1, J_2, J_3) \equiv (E; C)$, their two-dimensional anomalous dimensions $h(\sqrt{\lambda}, \hat{C})$ and their correlation functions. The marginality condition, identifying the physical states of the corresponding string theory, determines the energy of the state – or the dimension of the dual $\mathcal{N} = 4$ super-Yang-Mills (sYM) theory operator – in terms of its charges and the 't Hooft coupling, $E = \Delta = E(\sqrt{\lambda}, C)$. In the static gauge the string energy E has the more direct worldsheet interpretation as the worldsheet energy.

The complete worldsheet theory is classically integrable [1]; together with the integrability of the planar dilatation operator of the dual gauge theory this suggests that the worldsheet theory is integrable at finite values of the coupling.¹ Assuming all-orders integrability Asymptotic Bethe Equations (ABA) [4], Thermodynamic Bethe Ansatz (TBA) equations [5] and TBA equations in Y-variables [6] have been formulated for the spectrum of target space energies of long and general string states, respectively.

A remarkable feature of the worldsheet fluctuations around the BMN vacuum is that their exact dispersion relation

$$\epsilon^2 = 1 + \frac{\lambda}{\pi^2} \sin^2 \frac{\pi p_{\text{ws}}}{\sqrt{\lambda}} \quad (1.1)$$

bears a distinct similarity with that of a scalar particle on a space with a discrete space-like direction (with spacing $a = 2\pi/\sqrt{\lambda} = 1/2g$) with the important difference that *a priori* the momentum p_{ws} is not discrete. While this structure is not immediately manifest on the worldsheet and its consistency has been checked only in certain limits [7, 8, 9], it can be derived from various perspectives in the dual gauge theory [10, 11, 12].

The integrability-based predictions for the energies of certain long strings and long operators (*i.e.* strings/operators carrying at least one large quantum number) have been tested through four loops at weak gauge theory coupling [13, 14] and through two loops at strong coupling (weak worldsheet coupling expansion) [15, 16]. For short strings and short operators, the results of TBA/Y-system equations [17, 18] have been confirmed through five loops at weak gauge theory coupling [19] and through one loop at strong coupling [20, 21, 22]. While extensive and quite suggestive that integrability does indeed hold to all orders, such tests cannot definitively answer questions like:

1. Is it the target space energy operator that is diagonalized by the Bethe ansatz or is it another operator that differs from it at finite coupling or at sufficiently high order in weak/strong coupling perturbation theory?
2. Strong coupling perturbation theory is at best an asymptotic series which in certain cases [23] is known not to be Borel summable; is it possible to recover the weak gauge

¹Classical integrability was also shown in the pure spinor formalism in [2]; in [3] it was argued that the theory is also quantum-integrable.

theory coupling results for anomalous dimensions of local gauge-invariant operators from worldsheet calculations?

3. The worldsheet theory should be a finite quantum field theory; how sensitive are the results obtained in this theory on the regularization scheme?
4. How can one find the target space energy of short string states that cannot be (formally) described as limits of classical string solutions but rather have only a description in terms of vertex operators (*e.g.* chargeless states)?

Our aim in the present paper is to initiate the exploration of discrete approaches to the Green-Schwarz string in $\text{AdS}_5 \times \text{S}^5$. Using techniques of lattice field theory² to evaluate numerically the energy of a particular long string state at finite values of the 't Hooft coupling, in this paper we shall present evidence that the answers to the first two questions above are positive. While we shall not explicitly address the scheme dependence of the worldsheet calculations, we shall see that our results are consistent with the scheme chosen in worldsheet perturbative calculations. We shall also describe strategies for finding the spectrum of generic string states both in this framework as well as in worldsheet perturbation theory.³

Lattice field theory [30] is used extensively to study certain finite-coupling aspects of QCD as well as of condensed matter systems that can be analyzed in Euclidean setting. One constructs a discrete action on a four-dimensional square lattice which in the continuum limit becomes the desired action and evaluates the path integral numerically through Monte Carlo techniques. The partition function is arguably the simplest quantity to evaluate. Discrete forms of operators can also be placed on the lattice and the corresponding path integral yields their correlation functions. Here we will follow this strategy, discuss possible square-lattice discretizations of the Green-Schwarz string in $\text{AdS}_5 \times \text{S}^5$ and describe calculations that yield (in principle) quantities of interest for the dual gauge theory.

The properties of the theory are both a source of simplifications and complications. On the one hand, all fields are scalars (albeit some of them are anticommuting⁴) so their discretization is to some extent straightforward. On the other, Grassmann-odd fields can appear more than quadratically. Since it is difficult to simulate numerically anticommuting fields, they are usually integrated out; here however it is necessary to first linearize the terms that are more than quadratic and this potentially leads to a proliferation of auxiliary fields. Calculations then proceed by integrating out the Grassmann-odd fields and exponentiating the resulting determinant such that the number of propagating fields in the continuum limit is correct. Absence of anomalies makes this more straightforward than in four dimensions.

To illustrate the discrete approach to the Green-Schwarz string in $\text{AdS}_5 \times \text{S}^5$ we shall evaluate the energy of the long folded string for $1 \leq g \leq 40$ by computing the partition function of

²In the context of the gauge/string duality lattice field theory was used to study the Plane Wave Matrix Model [24] and the 16-supercharge 0 + 1-dimensional sYM theory [25]. Two-dimensional sigma models were studied in [26].

³Discrete approaches to the worldsheet theory have been proposed [27] as a systematic means of identifying the perturbation theory of the target space effective field theory from a worldsheet standpoint. In the context of the AdS/CFT correspondence this approach has been discussed in [28, 29].

⁴From this perspective these fields resemble the topologically-twisted fermions proposed in [31] as a way to realize supersymmetric field theories on the lattice, see [32] for a review.

the discretized AdS light-cone gauge action in the background of the null cusp solution; we reproduce within reasonable accuracy the results of the BES equation. This is the first finite-coupling calculation in this theory using field theory methods. We shall use the standard Rational Hybrid Monte Carlo (RHMC) algorithm [33, 34, 35] for an efficient treatment of the fermion determinant contribution (R) and for the evaluation of the path integral (HMC).

We begin in section 2 with a discussion on the discretization of the various forms of the Green-Schwarz action and brief comments on Monte Carlo methods for the evaluation of path integrals while relegating more details to Appendix A. We also outline three possible approaches to determining the worldsheet spectrum and other interesting quantities from numerical calculations. In section 3 we discuss in detail the example of the calculation of the universal scaling function. We outline the construction of the discrete version of the AdS light-cone action in the null cusp background and point out the discrete derivative required for a stable fermionic contribution, illustrate the evaluation of the partition function for one value of the coupling constant, discuss the dominant source of errors in the simulation and present our results. In section 4 we summarize our conclusions.

2 A numerical approach to the Green-Schwarz string

Lattice field theory provides a means to evaluate observables of the Green-Schwarz string in $\text{AdS}_5 \times \text{S}^5$ that are accessible on a Euclidean worldsheet, such as energies of string states or dimensions of the dual gauge-invariant operators, correlation functions of worldsheet operators, expectation values of Wilson loops, *etc.* In this section we discuss general features of possible approaches to the discretization of the Green-Schwarz action in $\text{AdS}_5 \times \text{S}^5$ as well as review and extend possible approaches to the calculation of target space energies of string states that may be implemented in this framework.

2.1 A first pass at a discrete Green-Schwarz action in $\text{AdS}_5 \times \text{S}^5$

To simulate a quantum field theory on a Euclidean lattice one begins with the continuum Euclidean action and discretizes it in a way that preserves as many of the continuum symmetries as possible. Lattice fields are assigned to either links (such as gauge fields) or to nodes (such as scalar fields). Under gauge transformations the link variables transform non-locally, depending on the beginning and end of the link, *e.g.* $L_{n,m} \mapsto U_n L_{n,m} U_m^\dagger$ while the node variables transform locally. Further considerations in the construction of the discrete action is the error introduced by the finite size lattice and the speed of the convergence of the continuum limit, the restoration of broken symmetries in the continuum limit, the existence of nontrivial renormalization and in particular of quantum-generated terms proportional to inverse lattice spacing which spoil the properties of the classical continuum limit, the proper treatment of fermions, the reality of the fermion contribution to the partition function (known as the fermion sign/phase problem [36]), the existence of anomalies and the solution to the fermion doubling problem *etc.*

Many of the issues present in standard matter-coupled gauge theories are absent in the Green-Schwarz string in curved space ⁵. For example, from the worldsheet standpoint all fields are

⁵This is true also in flat space, but that theory is effectively free.

scalars and thus they are uniformly assigned to lattice sites. Also, for a real bosonic background the fermionic contribution to the partition function is real and consequently there cannot be a phase ambiguity. Moreover, since the worldsheet theory is expected to be finite (and conformal in an appropriate gauge) one does not expect that renormalization is necessary and thus no counterterms need to be included in the action; however, composite operators whose correlation functions we may be interested in computing should receive infinite normalization so they should require counterterms. Last but not least, no two-dimensional anomalies are present and thus the doubling problem of fields with linear quadratic terms can be resolved without resorting to the usual four-dimensional techniques (see *e.g.* [37] for an introductory review).

The fact that κ symmetry is different from a standard gauge symmetry – in that it acts nonlinearly and does not have an independent gauge field – suggests that it must be treated differently from usual local symmetries. A possible approach – which we will adopt here and use in the explicit calculation in section 3 – is to discretize the gauge-fixed action. Since κ symmetry is related to worldsheet supersymmetry such an approach potentially breaks it. One may however test whether this is the case and, if necessary, correct for such effects.

There are several (classes of) actions that one might consider as the starting point for the construction of a lattice action:

1. Poincaré patch conformal gauge actions are typically simpler but they require the presence [38, 39, 40] of an extended string background. One may in principle avoid this by choosing a light-cone type κ -symmetry gauge while maintaining conformal gauge for two-dimensional diffeomorphisms. While the resulting action cannot be used for perturbative calculations (unless one further chooses a bosonic background) due to the absence of a free-fermion quadratic term, it may nevertheless be useful for lattice calculations.
2. Actions in which all constraints are solved are an appealing starting point for a construction of a discrete action as one needs not worry about the restoration of the corresponding symmetries in the continuum limit. Examples are the AdS-light-cone gauge [41] and the uniform light-cone gauge [42] actions⁶.
3. One may consider discrete projective light-cone gauge actions already put forward in the literature [27, 29, 28].

The appropriate choice depends on the observable to be computed and on the computational strategy. In the next subsection we will discuss approaches to the calculation of target space energies that make use of the first two types of actions and in section 3 we will use a discretized AdS-light-cone action.

The discretization of the bosonic action is straightforward: since all fields are scalars they are assigned to lattice sites

$$\phi(\tau, \sigma) \mapsto \phi_{(m,n)} \tag{2.1}$$

⁶Technical difficulties may arise in the latter case due to the Nambu square-root form of the uniform light-cone gauge action.

and their derivative in the direction of a unit two-dimensional vector \vec{v} is replaced by a finite difference

$$\partial_{\vec{v}}\phi \mapsto \frac{1}{a}(\phi_{(m,n)+\vec{v}} - \phi_{(m,n)}) , \quad (2.2)$$

where a is the lattice spacing. The error introduced by this replacement is $\mathcal{O}(a)$; depending on the desired precision for the calculation more involved discrete approximations for the continuum derivatives may be necessary. In Appendix B we include details on a nine-point approximation used in the calculation in section 3.

A common treatment of Grassmann variables is to integrate them out analytically; if higher-point fermion interactions are present they are first linearized by introducing an appropriate set of auxiliary fields auxiliary fields. The resulting determinant is either evaluated directly or exponentiated in terms of commuting pseudo-fermions,

$$\int D\Psi e^{-\int d^2\xi \psi M \psi} = (\det M)^{1/2} = (\det MM^\dagger)^{1/4} = \int D\zeta D\bar{\zeta} e^{-\int d^2\xi \bar{\zeta}(MM^\dagger)^{-1/4}\zeta} . \quad (2.3)$$

In general, care must be taken to avoid double-counting the fermionic contribution in the continuum limit. In our case one can show that the Pfaffian of M is real and thus it is sufficient to exponentiate the operator MM^\dagger ; since it contains a Klein-Gordon operator (in general up to a field-dependent prefactor which is expected to effectively acquire a vacuum expectation value), its discretization is similar to that of regular commuting scalars and is free of unwanted doublers [43].

The strategy for computing correlation functions in lattice field theory is to approximate the path integral in terms of finitely many field configurations which sample the entire phase space. A very efficient algorithm for generating these field configurations is the RHMC algorithm [33, 34, 35], which we shall review in some detail in Appendix A. With a specific rational approximation for the fractional power of the fermion matrix (2.3), one defines an evolution Hamiltonian ⁷ by adding to the discrete action the squared conjugate momentum for each field, randomly generates some field configuration and then generates further ones by repeating the following steps:

1. randomly generates momenta for all fields from a Gaussian distribution
2. evolves the field configuration with the evolution Hamiltonian (Molecular dynamics) for some “time” interval $\Delta\tau$
3. accepts the initial or the final field configuration stochastically, through a Metropolis acceptance test (which, in some sense, “decides” whether the final field configuration can be the result of a quantum mechanical evolution). This step eliminates errors introduced at step 2) due to various approximations.

It has been shown in [33] that this algorithm leads to field configurations which cover the entire phase space of the system and can be used to construct the partition function or correlation functions of operators.

⁷This Hamiltonian is the evolution operator along some fictitious (Monte Carlo) “time” direction τ .

2.2 Various approaches to energy calculations

The semiclassical expansion has been extensively used to study the worldsheet perturbative expansion of energies of long strings in $\text{AdS}_5 \times \text{S}^5$ – *i.e.* strings with large quantum numbers and thus dual to long sYM operators with large canonical dimensions (see *e.g.* [44] for a review). It was suggested in [45] that similar techniques may also be applied to short strings, provided that the corresponding state can be obtained by analytic continuation from a long string state. A strategy that uses the conformal dimension of worldsheet vertex operators and potentially yields the energy of generic string states, has been discussed in [46]. Here we briefly review these techniques and add another one based on the worldsheet construction of two-point functions of local gauge theory operators and phrase them such that they are amenable to numerical calculations based on discretized worldsheet actions in $\text{AdS}_5 \times \text{S}^5$.

2.2.1 A conformal gauge approach

In conformal gauge the worldsheet theory for strings in $\text{AdS}_5 \times \text{S}^5$ is a conformal field theory – albeit one which is neither factorizable nor particularly suited to a perturbative treatment due to the special features of the Green-Schwarz fermions. Conformal invariance determines the form of the two-point function of local worldsheet operators; using it we may extract target space information from a (direct numerical) evaluation of the two-point function of fairly general local worldsheet operators.

Indeed, a general local operator $W(\xi)$ can be expanded in the basis of local operators with definite worldsheet dimension h_n as

$$W(\xi) = \sum_n c_{W,n} V_n(\xi) . \quad (2.4)$$

The general form of the two-point function of the basis elements

$$\langle V_m(\xi_1) V_n(\xi_2) \rangle = \delta_{m,n} \frac{c_V}{|\xi_1 - \xi_2|^{2h}} \quad (2.5)$$

implies that the two-point function $\langle W(\xi_1) W(\xi_2) \rangle$ is

$$\langle W(\xi_1) W(\xi_2) \rangle = \sum_n \frac{c_n c_{W,n}^2}{|\xi_1 - \xi_2|^{2h_n}} , \quad (2.6)$$

where the normalization factor c_V and the conformal dimensions h_n depend on the worldsheet coupling constant and the charges of the operator V_n under various target space symmetries. Assuming some way of determining the worldsheet two-point function of two operators $W(\xi)$, the lowest worldsheet conformal dimension that appears in (2.6) may be extracted from the large distance asymptotics. More generally, given a sufficiently precise determination of $\langle W(\xi_1) W(\xi_2) \rangle$, the dimensions h_n of other vertex operators that enter the decomposition (2.4) may in principle be extracted through a Fourier analysis; the coefficients c_n and $c_{W,n}$ need not be known.

Then, the condition that V_n are exactly marginal,

$$h_n = 2 , \quad (2.7)$$

determines the target space energy of the corresponding string state in terms of its charges and the 't Hooft coupling.

To carry out such a program it is useful to choose an operator W with definite charge under the target space symmetries which also depend explicitly on the target space energy or boundary conformal dimension; the classical bosonic vertex operators discussed in conformal gauge in [47, 48, 46] are possible candidates. As discussed in section 2, from the perspective of a numerical calculation of the two-point function (2.6), purely bosonic approximate vertex operators are very useful because fermions can be integrated out analytically. Bosonic vertex operators are naturally constructed in terms of the embedding coordinates

$$Y_a Y^a = Y_+ Y_+^* - Y_x Y_x^* - Y_y Y_y^* = 1, \quad Z_k Z_k = Z_x Z_x^* + Z_y Z_y^* + Z_z Z_z^* = 1, \quad (2.8)$$

where $Y_+ = Y_0 + iY_5$, $Y_x = Y_1 + iY_2$, $Y_y = Y_3 + iY_4$, $Z_x = Z_1 + iZ_2$, $Z_y = Z_3 + iZ_4$, $Z_z = Z_5 + iZ_6$ and the relation to the Poincaré patch is the usual one

$$Y_m = \frac{x_m}{z}, \quad Y_4 = \frac{1}{2z}(-1 + z^2 + x^m x_m), \quad Y_5 = \frac{1}{2z}(1 + z^2 + x^m x_m). \quad (2.9)$$

In the embedding coordinates the conformal gauge bosonic action is

$$S = \frac{\sqrt{\lambda}}{4\pi} \int d^2\sigma \left(-\partial Y_a \cdot \partial Y^a + \partial Z_k \cdot \partial Z_k + \text{fermions} \right). \quad (2.10)$$

To describe vertex operators it is useful to do a Euclidean rotation both on the worldsheet and in the target space

$$t_e = it, \quad Y_{0e} = iY_0, \quad x_{0e} = ix_0, \quad (2.11)$$

so that $Y^M Y_M = -Y_5^2 + Y_{0e}^2 + Y_i Y_i + Y_4^2 = -1$. Then, unintegrated vertex operators have the form

$$V \sim (Y_+)^{-\Delta} \left[(\partial^s Y)^r \dots (\bar{\partial}^m Z)^n + \dots \right] \equiv (Y_+)^{-\Delta} U(Y, Z, \dots). \quad (2.12)$$

where

$$K(x, z) = k_\Delta (Y_+)^{-\Delta} = k_\Delta (z + z^{-1} x^m x_m)^{-\Delta}, \quad \text{and} \quad Y_+ \equiv Y_5 + Y_4 \quad (2.13)$$

is the usual bulk-to-boundary propagator in AdS space. ⁸

On a discrete worldsheet the unintegrated vertex operator is placed at a lattice site

$$V(\xi) \mapsto V_{(m,n)} \quad (2.14)$$

and depends on as many adjacent sites as are used to define the discrete derivative of a field (the number of such derivatives appearing in V is related to the string level). The two-point function of such operators (specified by the parameter Δ and a choice of $U(Y, Z, \dots)$)

$$\langle V_{(m_1, n_1)} V_{(m_2, n_2)} \rangle = \frac{1}{Z} \int D[x_{(m,n)}, z_{(m,n)}^M, \theta_{(m,n)}, \eta_{(m,n)}] e^{-S_{\text{discrete}}} V_{(m_1, n_1)} V_{(m_2, n_2)} \quad (2.15)$$

⁸As explained in [47, 48], the structure of the vertex operator follows closely that of flat space vertex operators, with $(Y_+)^{-\Delta}$ being the Euclidean analog of e^{-iEt} and $U(Y, X, \dots)$ carrying the dependence on the string level, symmetry transformations, *etc.*

may then be computed through Monte Carlo techniques which we will review in Appendix A as a function of Δ , the symmetry charges, the worldsheet coupling and the lattice separation $d_{12}^2 = ((m_1 - m_2)^2 + (n_1 - n_2)^2)$.⁹ Extracting from it the worldsheet conformal dimensions h_n (or perhaps only the smallest one)¹⁰ as a function of Δ , λ and identifying the curve with the equation (2.7) yields the target space energy $\Delta = \Delta(\lambda, \dots)$.

Since the discrete action is not conformally invariant, the extraction of the worldsheet conformal dimensions h_n requires a careful consideration of the continuum limit.¹¹ In turn, the curve with equation (2.7) yields the target space energy $\Delta = \Delta(\lambda, \dots)$.

By not imposing the Virasoro constraint from the outset as well as by not focusing from the outset on target space quantities, the outcome of this algorithm potentially provides us with a wealth of information on conformal field theories of Green-Schwarz type. For the goal of finding the energies of string states these features make it however computationally intensive due to the large number of intermediate steps necessary to find Δ from the worldsheet two-point function. It is therefore important to identify strategies that require fewer/simpler auxiliary quantities.

2.2.2 Operator dimensions from the boundary two-point functions

Integrated vertex operators [48, 49], labeled by a point on the boundary of AdS space, are dual to local gauge-invariant operators of the boundary theory. They provide a means to construct the two-point function of general local operators in the boundary theory from which one may extract directly the eigenvalues of the dilatation operator.

A general local gauge-invariant operator $O(x)$ in the boundary theory can always be decomposed in a basis of local operators $\mathcal{O}_n(x)$ with definite (anomalous) dimensions

$$O(x) = \sum_n c_{O,n}(\lambda) \mathcal{O}_n(x) . \quad (2.16)$$

Using the form of the two-point functions of $\mathcal{O}_n(x)$ dictated by conformal invariance,

$$\langle \mathcal{O}(x) \mathcal{O}(y) \rangle = \frac{c_{\mathcal{O}}(\lambda)}{|x - y|^{2\Delta_{\mathcal{O}}}} , \quad (2.17)$$

⁹In computing this correlation function it may be necessary to add to $V_{(m,n)}$ counterterms proportional to the inverse lattice spacing; this is due to the fact that in the continuum theory operators are expected to receive infinite renormalization responsible for their two-dimensional anomalous dimension.

¹⁰It is possible to argue that, in the context of our discussion, one can unambiguously follow one worldsheet dimension from weak to strong worldsheet coupling. Indeed, it was suggested in [47] that the dimensions of gauge theory operators obey a non-intersection principle – *i.e.* that there should be no level crossings for states with the same quantum numbers as λ changes from small to large values. Then, the general structure of the worldsheet anomalous dimension [48, 46]

$$h_n = \Delta_n(\Delta_n - c) + F_n(\sqrt{\lambda}, Q) ,$$

together with the positivity of Δ and h imply that the worldsheet (anomalous) dimensions should also obey a non-intersection principle.

¹¹It is possible that the leading term in the large distance expansion is less sensitive to the details of the discretization and may be used to extract the smallest worldsheet dimension even on a finite-size lattice.

($c_{\mathcal{O}}(\lambda)$ is a potentially nontrivial normalization factor) it follows that the two-point function of the operators $\mathcal{O}(\mathbf{x})$ is

$$\langle \mathcal{O}(\mathbf{x})\mathcal{O}(\mathbf{y}) \rangle = \sum_n \frac{c_n(\lambda)c_{\mathcal{O},n}^2(\lambda)}{|\mathbf{x} - \mathbf{y}|^{2\Delta_n}} . \quad (2.18)$$

Thus, assuming that it is possible to find the exact two-point function of $\mathcal{O}(\mathbf{x})$, it is then possible to extract the dimensions of the operator of lowest dimension in its spectral decomposition (2.16) from the large-distance behavior of the two-point function (2.18); the dimensions of the other operators in (2.16) may also be extracted through a Mellin transform or by simply fitting the two-point function to an expression of the type (2.18).

It is in general difficult to identify the vertex operator corresponding to a specified gauge theory operator; to carry out the program above however it suffices to know the two-point function of *some* operator \mathcal{O} . Thus, one can simply pick any desired integrated vertex operator $V(\mathbf{x})$ and, if its two-point function can be computed, it can in principle be used to extract the dimension of the gauge theory operators with nonvanishing overlap with its dual \mathcal{O}_V . It is intuitively clear that, to extract information from a numerical (and thus inherently not exact) evaluation of the two-point function $\langle V(\mathbf{x})V(\mathbf{y}) \rangle$, it is useful to have as few dominant terms as possible on the right-hand side of eq. (2.18). One may, of course, target operators with a specific PSU(2, 2|4) quantum numbers $\mathbf{C} = (S_1, S_2; J_1, J_2, J_3)$ by choosing a worldsheet operator with the same charges.¹² Further super-selection sectors are introduced by the gauge theory engineering dimension and the string level. At least at small and large 't Hooft coupling they guarantee that the dimensions Δ differ by $\mathcal{O}(1)$ and $\mathcal{O}(\lambda^{1/4})$ quantities respectively and thus the features of the two-point function are expected to be well-separated in Mellin space.

The integrated vertex operator associated to the unintegrated vertex operator (2.12) is [48, 49]

$$V(\mathbf{x}) = \int d^2\xi V(x(\xi) - \mathbf{x}; \dots) = \int d^2\xi [K(x(\xi) - \mathbf{x}, z(\xi))]^{-\Delta} U[x(\xi) - \mathbf{x}, Z(\xi)] ; \quad (2.19)$$

Its form on the discrete worldsheet is obtained by using the discrete fields and replacing the integral with a sum over all lattice sites,

$$V(\mathbf{x}) = \frac{1}{a^2} \sum_{m,n} V_{(m,n)}(x_{(m,n)} - \mathbf{x}; \dots) . \quad (2.20)$$

The boundary two-point function of the dual operator $\mathcal{O}_V(\mathbf{y})$ is then given by

$$\langle \mathcal{O}_V(\mathbf{x})\mathcal{O}_V(\mathbf{y}) \rangle = \langle V(\mathbf{x})V(\mathbf{y}) \rangle = \frac{1}{Z} \int D[x_{(m,n)}, z_{(m,n)}^M, \theta_{(m,n)}, \eta_{(m,n)}] e^{-S_{\text{discrete}}} V(\mathbf{x})V(\mathbf{y}) \quad (2.21)$$

and, as in the case of the two-point function in the previous section, may then be computed through Monte Carlo techniques.¹³

¹²Operators with identical charge vectors \mathbf{C} may be further distinguished by hidden local charges such as those related to the integrable structure of the planar theory.

¹³The comments as in footnote 9 apply to this calculation as well.

For each value of the 't Hooft coupling this algorithm requires the evaluation of a single auxiliary function of one variable – the boundary separation of operators $|x_1 - x_2|$ – and the dimensions of operators in the boundary theory follow directly from it. This two-point function may be computed either with a discretized conformal gauge action or with a discretized action in a physical gauge, such as the light-cone gauge. In the latter case however it may be useful to choose a slightly different worldsheet operator $V(x)$ than described above.

Indeed, in this gauge one of the Cartan generators of the boundary rotation group is spontaneously broken and thus it cannot be used to label V . Moreover, the worldsheet field x^- is nonlocal (with local derivatives) and thus not easy to use as an argument of V in eq. (2.19). A straightforward resolution is to simply not include the bulk-to-boundary factor K in V and choose a function U which depends on x^\pm only through their derivatives:

$$V_{\text{lc}}(x_\perp) = \int d^2\xi U[x_\perp(\xi) - x_\perp, Z(\xi)] \rightarrow \sum_{m,n} U_{(m,n)}(x_{\perp,(m,n)} - x_\perp; \dots) . \quad (2.22)$$

While this cannot be called “vertex operator”, it is nevertheless dual to some local boundary operator labeled by the two coordinates x_\perp transverse to the light-cone. Interpreting the absence of x^\pm as they having been set to zero, the dimensions of operators in the boundary theory may be extracted from an expansion analogous to eq. (2.18) which now depends only on $|x_{\perp,1} - x_{\perp,2}|$.

2.2.3 Target space energy from a partition function

The time-honored approach to perturbative calculations of worldsheet quantum corrections to the energy of long string states is as the worldsheet vacuum energy in the background of the classical solution describing the state [50] (see [44] for a review and a complete list of references). It has been argued in [51] and further elaborated on in [52, 16] that, for single-charge string states, this is also the worldsheet free energy. More precisely, for single-charge solutions for which the AdS global time is related to the worldsheet time as $t = \kappa\tau$ the target space energy is also given by

$$E = -\frac{1}{\kappa} \ln Z . \quad (2.23)$$

More involved expressions relate the partition function and the energy of multi-charge states for which all parameters may be interpreted as chemical potentials for various charges [52, 16]. It was moreover argued in [46, 20, 21, 22] that similar semiclassical techniques capture correctly the energy of short string states which can be interpreted as the small charge continuation of long string states.

The evaluation of the partition function of a theory is arguably the simplest lattice field theory calculation and thus provides a good testing ground for the applicability of this framework to the Green-Schwarz string. Thus, a strategy – which we will illustrate in section 3 – is to first find the complete continuum action of fluctuations $\tilde{\Phi}$ around the desired classical solution Φ_{cl} and discretize it as discussed in sec. 2.1.¹⁴ As before, the action $S_{E,\text{discrete}}$ is the sum over all

¹⁴A *priori* this action may exhibit position dependence inherited from the classical background (if the classical solution is inhomogeneous). This simply translates into an explicit dependence of the Lagrangian on the lattice site (and on the lattice spacing) apart from that of fields.

lattice sites of the discrete Lagrangian. Then we evaluate the partition function

$$Z = \int D\Phi_{(m,n)} e^{-S_{E,\text{discrete}}} \quad (2.24)$$

as a function of the parameters of the solution (*i.e.* for many choices of those parameters and then construct an interpolating function) and the 't Hooft coupling; from it one extracts the energy of the corresponding string state either through (2.23) or through the more involved relations derived in [52, 16].

This approach should be insensitive to the details (such as gauge choices) of the continuum action. However, only long string states whose Euclidean action is real can be considered; this is due to the fact that, in the Monte Carlo evaluation of path integrals, the corresponding probability measure, $\exp(-S_E)$, is required to be real. Many interesting solutions – such as the spin- S folded string (with and without angular momentum on S^5), various circular string solutions whose analytic continuation to small charges describe members of the Konishi multiplet, *etc.* – satisfy these restrictions. In the next section we discuss in detail an application of this strategy.

3 An example: the universal scaling function at finite coupling

The universal scaling function is expected to be the solution to the BES equation; this equation reproduces the first few orders in the weak [13, 14] and strong [51, 15] coupling expansions that have been computed directly:

$$f(\lambda)|_{\lambda \rightarrow 0} = 8g^2 \left[1 - \frac{\pi^2}{3}g^2 + \frac{11\pi^4}{45}g^4 - \left(\frac{73}{315} + 8\zeta_3 \right) g^6 + \dots \right] \quad (3.1)$$

$$f(\lambda)|_{\lambda \rightarrow \infty} = 4g \left[1 - \frac{3 \ln 2}{4\pi g} - \frac{K}{16\pi^2 g^2} + \dots \right], \quad g = \frac{\sqrt{\lambda}}{4\pi}. \quad (3.2)$$

Further terms in these expansions as well as the value of the universal scaling function at finite values of the coupling can be obtained from the BES equation¹⁵. We will reproduce these values (within numerical errors) at various values of $g \in [1, 40]$ by numerically evaluating the worldsheet partition function in the background of the null cusp solution. Smaller values of g , inside the radius of convergence of sYM perturbation theory are, in principle accessible but are currently limited by the accuracy of our simulation.

We take the continuum worldsheet theory to be given by AdS-light-cone gauge action Wick-rotated to a Euclidean worldsheet [41, 15]:

$$S = g \int dt \int_0^\infty ds \mathcal{L}_E, \quad (3.3)$$

$$\begin{aligned} \mathcal{L}_E = & \dot{x}^* \dot{x} + (\dot{z}^M + iz^{-2} z_N \eta_i \rho^{MNi} \eta^j)^2 + i(\theta^i \dot{\theta}_i + \eta^i \dot{\eta}_i - h.c.) - z^{-2} (\eta^2)^2 \\ & + z^{-4} (x'^* x' + z'^M z'^M) + 2i \left[z^{-3} \eta^i \rho_{ij}^M z^M (\theta'^j - iz^{-1} \eta^j x') + h.c. \right]. \end{aligned} \quad (3.4)$$

¹⁵While strong coupling perturbation theory is not summable, the first three terms in this expansion are a good numerical approximation to the exact function for $g \geq 1$

It has manifest $U(1) \times SO(6) \simeq U(1) \times SU(4)$ symmetry. The fermions are complex $\theta^i = (\theta_i)^\dagger$, $\eta^i = (\eta_i)^\dagger$ ($i = 1, 2, 3, 4$) and transform in fundamental representation of $SU(4)$; the matrices ρ_{ij}^M are the off-diagonal blocks of six-dimensional gamma matrices in chiral representation and $(\rho^{MN})_i^j = (\rho^{[M} \rho^{\dagger N]})_i^j$ and $(\rho^{MN})^i_j = (\rho^{\dagger[M} \rho^{N]})^i_j$ are the $SO(6)$ generators. The fields z^M are neutral under $U(1)$, θ^i and η^i have opposite charges and the charge of η_i is half the charge of x .

3.1 The null cusp fluctuation action, discretization, and some numerical details

The classical solution of (3.4) dual to the null cusp and the action for fluctuations around it were constructed in [15] (\tilde{z} is the norm of the six-component fluctuation vector \tilde{z}^M):

$$\begin{aligned}
\mathcal{L}_{\text{cusp}} &= |\partial_t \tilde{x} + \frac{1}{2} \tilde{x}|^2 + \frac{1}{\tilde{z}^4} |\partial_s \tilde{x} - \frac{1}{2} \tilde{x}|^2 \\
&+ (\partial_t \tilde{z}^M + \frac{1}{2} \tilde{z}^M + \frac{i}{\tilde{z}^2} \tilde{\eta}_i (\rho^{MN})^i_j \tilde{\eta}^j \tilde{z}_N)^2 + \frac{1}{\tilde{z}^4} (\partial_s \tilde{z}^M - \frac{1}{2} \tilde{z}^M)^2 \\
&+ i(\tilde{\theta}^i \partial_t \tilde{\theta}_i + \tilde{\eta}^i \partial_t \tilde{\eta}_i + \tilde{\theta}_i \partial_t \tilde{\theta}^i + \tilde{\eta}_i \partial_t \tilde{\eta}^i) - \frac{1}{\tilde{z}^2} (\eta^2)^2 \\
&+ 2i \left[\frac{1}{\tilde{z}^3} \tilde{\eta}^i (\rho^M)_{ij} \tilde{z}^M (\partial_s \tilde{\theta}^j - \frac{1}{2} \tilde{\theta}^j - \frac{i}{\tilde{z}} \tilde{\eta}^j (\partial_s x - \frac{1}{2} x)) \right. \\
&\quad \left. + \frac{1}{\tilde{z}^3} \tilde{\eta}_i (\rho_M^\dagger)^{ij} \tilde{z}^M (\partial_s \tilde{\theta}_j - \frac{1}{2} \tilde{\theta}_j + \frac{i}{\tilde{z}} \tilde{\eta}_j (\partial_s x^* - \frac{1}{2} x^*)) \right].
\end{aligned} \tag{3.5}$$

As discussed there, the universal scaling function is proportional to the worldsheet free energy

$$Z_{\text{string}} = e^{-W(g)} \quad , \quad W(g) = \frac{1}{2} f(\lambda) \mathcal{V} = \frac{1}{8} f(\lambda) \int dt \int ds \, 1 \quad . \tag{3.6}$$

The various numerical factors are related to the coordinate transformation and field redefinition between the long folded (GKP) string in global AdS coordinates and the null cusp solution in the Poincaré patch in light-cone gauge [15].

To integrate out the fermions the quartic terms are linearized by introducing a scalar and an $SO(6)$ vector auxiliary fields:

$$-\frac{1}{\tilde{z}^2} (\tilde{\eta}^2)^2 \mapsto \frac{1}{2} \tilde{\phi}^2 + \frac{\sqrt{2}}{\tilde{z}} \tilde{\phi} \tilde{\eta}^2 \quad , \quad -\frac{1}{\tilde{z}^4} (\tilde{z}_N \tilde{\eta} \rho^{MN} \tilde{\eta})^2 \mapsto \frac{1}{2} (\tilde{\phi}_M)^2 + \frac{\sqrt{2}}{\tilde{z}^2} \tilde{\phi}_M \tilde{z}_N \tilde{\eta} \rho^{MN} \tilde{\eta} \quad . \tag{3.7}$$

The resulting quadratic fermion matrix M_{cusp} can be read without difficulty; for completeness we include it in appendix C. Integrating out the fermions and exponentiating the resulting determinant leads to the action

$$\begin{aligned}
\mathcal{L} &= |\partial_t \tilde{x} + \frac{1}{2} \tilde{x}|^2 + \frac{1}{\tilde{z}^4} |\partial_s \tilde{x} - \frac{1}{2} \tilde{x}|^2 + (\partial_t \tilde{z}^M + \frac{1}{2} \tilde{z}^M)^2 + \frac{1}{\tilde{z}^4} (\partial_s \tilde{z}^M - \frac{1}{2} \tilde{z}^M)^2 \\
&+ \frac{1}{2} \tilde{\phi}^2 + \frac{1}{2} (\tilde{\phi}_M)^2 + \zeta^\dagger (M_{\text{cusp}}^\dagger M_{\text{cusp}})^{-1/4} \zeta \quad ;
\end{aligned} \tag{3.8}$$

it contains 15 real bosonic fields (8 physical and 7 auxiliary) as well as 16 more complex bosons ζ used to exponentiate the fermion determinant, cf. eq. (2.3)¹⁶.

¹⁶In that equation the formal variable ψ stands for $\psi \equiv (\tilde{\theta}^i, \tilde{\theta}_i, \tilde{\eta}^i, \tilde{\eta}_i)$ with $i = 1, \dots, 4$.

Its discretization, as reviewed in section 2.1, is relatively straightforward. Using the block structure of M_{cusp} (C.2) one can easily convince oneself that $M_{\text{cusp}}^\dagger M_{\text{cusp}}$ contains the Klein-Gordon operator as a free limit. As in the case of bosons its discrete version converges to the right continuum limit and is free of unwanted doublers. Moreover, its determinant is real and positive and thus its fourth-root is unambiguous. As described in Appendix A, we will approximate $(M_{\text{cusp}}^\dagger M_{\text{cusp}})^{-1/4}$ as a rational function of $(M_{\text{cusp}}^\dagger M_{\text{cusp}})$ [53]:

$$(M^\dagger M)^{-\frac{1}{4}} = \alpha_0 + \sum_{i=1}^P \frac{\alpha_i}{M^\dagger M + \beta_i} . \quad (3.9)$$

The standard choice $P = 15$ leads in our case to an error $\mathcal{O}(10^{-5})$ for $g \in (10^{-7}, 10^3)$.

In the discretization of the Lagrangian (3.8) we could, in principle, use the simplest two-site version of the discrete derivative (2.2), whose error is $\mathcal{O}(a)$. It turns out however that, for lattice sizes accessible to us this approximation is too coarse and leads to numerically-unstable fermion contributions. We found that stability is achieved only for an error of $\mathcal{O}(a^8)$. We must therefore use a nine point stencil for the derivative

$$\begin{aligned} a\partial_x f(x) &= \frac{4}{5}(f(x+a) - f(x-a)) - \frac{1}{5}(f(x+2a) - f(x-2a)) \\ &\quad + \frac{4}{105}(f(x+3a) - f(x-3a)) - \frac{1}{280}(f(x+4a) - f(x-4a)) + \mathcal{O}(a^9) . \end{aligned} \quad (3.10)$$

For completeness we include its derivation in Appendix B. It is also trivial to choose a discretization that preserves the manifest global $SO(6)$ symmetry of (3.8).

To construct the action (3.8) from the action in eq. (3.5) we introduced a number of Lagrange multiplier fields; to recover the original action one is to use the saddle-point approximation to integrate them out. While this is harmless in the continuum theory, strictly speaking the partition function of the original theory is recovered only up to factors of the determinant of the unit operator. While these factors are expected to be unity in the continuum theory, in the presence of a regulator they may be nontrivial, albeit coupling constant independent. Since the initial partition function is such that it equals unity if the action were zero, we will eliminate the potential extra factors by dividing by the partition function with $S_E = 0$. We have checked that the corresponding subtraction term in the free energy decreases as the lattice spacing is decreased, consistent with it being an artifact of the discretization.

Even though the original action (3.8) is defined on an infinite worldsheet, simulating it on a lattice requires placing it in finite volume. It has been suggested in [54] that the finite-size effects due to placing the theory on a cylinder of length L translate into $\delta f \sim 1/L^2$ corrections to the universal scaling function (and to $1/L = 1/\ln S$ corrections to the energy of the long folded string). It is easy to argue that such effects are of the same order as the minimal finite-volume error (if the lattice has equal sides) and thus cannot be extracted from a calculation of the type we will describe here.

To estimate a lower bound on the finite-volume effects vis-à-vis the fact that we are interested in the value of the (free) energy we use the uncertainly relations. Taking the time uncertainly to be the same as the length of the (Euclidian) time direction of our lattice, $\Delta t = T$, the

uncertainty in the energy is

$$\Delta E \geq \frac{1}{2T} . \quad (3.11)$$

By dividing out the length of the time direction in (3.6), the uncertainty in the energy is related to the uncertainty in the universal scaling function as

$$\Delta E = \frac{V_2}{8T} \Delta f(g) ; \quad (3.12)$$

It thus follows that the error on the universal scaling function is bounded from below by

$$\Delta f(g) \geq \frac{4}{V_2} . \quad (3.13)$$

Other sources – such as statistical, discretization, etc – add to this estimate. If the length of the space-like and Euclidian time-like direction are of the same order this error is of the same order as the expected finite volume correction to the universal scaling function, $\delta f \sim 1/L^2$. One may attempt to distinguish them by considering an asymmetric lattice with the time-like direction much larger than the space-like direction. We shall not pursue this here.

3.2 The simulation, data analysis and results

To simulate the discretized action (3.8) on a lattice we employed the RHMC algorithm reviewed in appendix A. We used¹⁷ 10×10 and 12×12 lattices with volume $V_2 = \pi^2$ and evaluated the worldsheet free energy W and the universal scaling function $f(g)$ (cf. eq. (3.6)) for several values of the coupling

$$g \in \{1, 2, 5, 10, 15, 20, 30, 40\} . \quad (3.14)$$

To avoid potential problems with constant spinors in the regime when fermions are effectively light¹⁸ we will use anti-periodic boundary conditions for fermions while all bosons are taken to be periodic. The fermion boundary conditions are captured by the detailed structure of the matrix $(M_{\text{cusp}}^\dagger M_{\text{cusp}})$ in the discretized theory and arises from the derivatives on fermions at the edges of the lattice. It is interesting to note that if the fermion boundary conditions are chosen to be periodic the simulation does not appear to converge.

The universal scaling function for each value of g is the result of an independent simulation. Following the RHMC algorithm [33, 34, 35] reviewed in Appendix A, field configurations are generated by starting with a random field configuration and evolving it along a fictitious time direction. At the end of every n_T -step "time" sequence¹⁹ the resulting field configuration

¹⁷The number of lattice sites and the lattice volume are chosen such that the simulation runs sufficiently fast while still having reasonably small discretization errors.

¹⁸This occurs at small values of the 't Hooft coupling: the free momentum space action looks like $S \sim g(p^2 + m^2)$; for fixed gp^2 the mass term is irrelevant at small values of g .

¹⁹The number of steps n_T and the length of each step are tunable parameters chosen to decrease the thermalization time, see Figure 1(a).

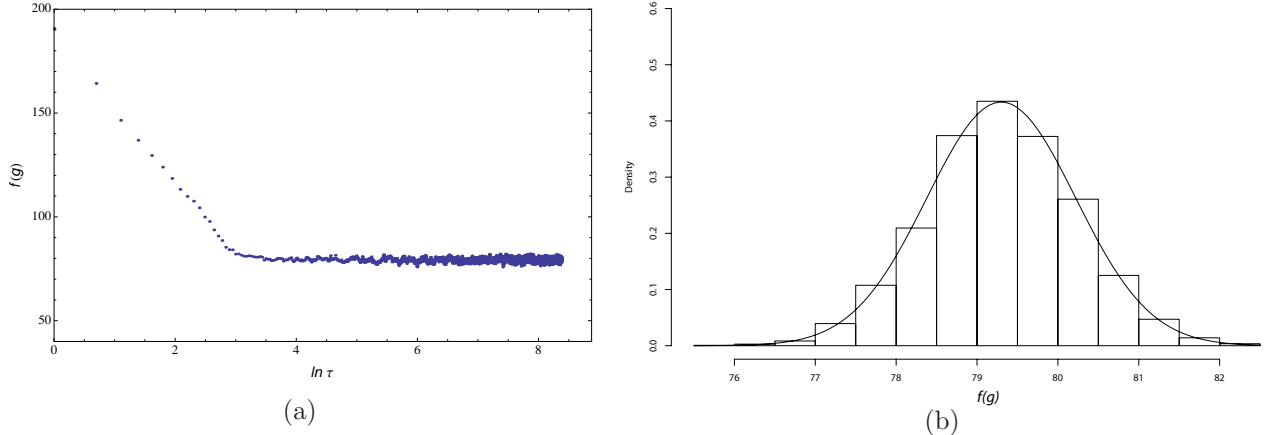


Figure 1: The value of the action as a function of the (logarithm of the) evolution time τ for $g = 20$ and the distribution at sufficiently late times. (a) The evolution of the value of the free energy along the Monte Carlo time. Each point represents the value of the free energy on the accepted field configuration at the end of each sequence of $n_T \simeq 10$ steps (an HMC trajectory). After some time (in this case $\ln \tau \sim 6$) the state “thermalizes”, *i.e.* the value of the free energy on the generated field configurations follow a normal distribution. (b) The value of the free energy and the corresponding error (and in fact of any other observable) is found by fitting a Gaussian on sufficiently many values after thermalization; the histogram is constructed from about 500 data points.

is kept or rejected whether or not it can be interpreted as the result of an actual quantum mechanical evolution of the system and momenta are re-generated. It was shown in [33] that the resulting field configurations sample the complete phase space of the system. After a sufficiently long evolution the values of the free energy (or of any other observable) follow a Gaussian distribution; the free energy and its error are extracted as the mean value and the standard deviation of this distribution, respectively. Figure 1(a) shows, for $g = 20$, the evolution of the value of the action along the evolution towards thermal equilibrium and figure 1(b) shows the corresponding Gaussian fit.²⁰

The results of the simulations of the action (3.8) on a 10×10 and 12×12 lattice are listed in the second and third two columns of table 1 and plotted in figures 2(a) and 2(b), respectively. On the scale of the plot the two data sets are practically indistinguishable. Inspecting the numerical values reveals small variations in the position of the central value as well as a reduction in their absolute errors. This reduction is consistent with the expectation that the discretization errors are smaller on finer lattices. In the fourth column of table 1 we include the values of the universal scaling function obtained by solving the BES equation for the same values of g .²¹

The sources of errors are well-understood, see Appendix A.5 for a brief summary. The lower

²⁰Here and for the other values of g we carry out the fit using the Maximum-likelihood Fitting of Univariate Distributions in the statistical data analysis package R [55]. See also <http://stat.ethz.ch/R-manual/R-devel/library/MASS/html/fitdistr.html>

²¹We thank D. Volin for a numerical solution of the BES equation.

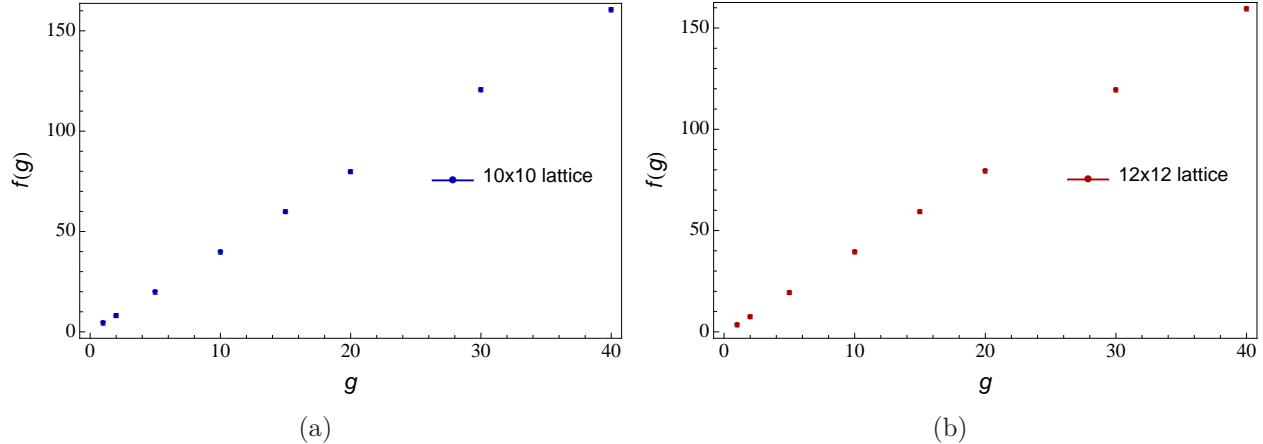


Figure 2: The universal scaling function for the values of g in eq. (3.14) from 10×10 and 12×12 lattice simulations.

g	10×10 lattice	12×12 lattice	BES equation
1	4.328 ± 0.97	$3.335 \pm .89$	3.3066
2	8.127 ± 0.96	$7.385 \pm .91$	7.3246
5	19.694 ± 0.92	$19.373 \pm .91$	19.3332
10	39.652 ± 0.92	$39.380 \pm .92$	39.3359
15	59.878 ± 0.93	$59.306 \pm .93$	59.3369
20	79.804 ± 0.95	$79.313 \pm .94$	79.3429
30	120.628 ± 1.00	$119.408 \pm .97$	119.4052
40	160.480 ± 1.05	$159.422 \pm .98$	159.5485

Table 1: The numerical values of the universal scaling function obtained from 10×10 and 12×12 lattices as well as the results of the BES equation. The latter are quoted with an uncertainty of one unit in the last digit.

bound on the finite volume error estimated in (3.13) becomes here

$$\Delta f(g) \geq \frac{4}{V_2} = \frac{4}{\pi^2} \simeq 0.4 . \quad (3.15)$$

This accounts for about 50% of the reported error in table 1. At large values of the coupling constant the extra error is statistically-dominated due to a slow thermalization time and low acceptance rate of the RHMC algorithm; this can presumably be justified by the fact that at large values of g the partition function is dominated by a single classical field configuration rather than by a distribution of field configurations. At small values of g the error induced by the fermion determinant provides the bulk of the extra error; this is a consequence of the fact that fermions become effectively light in this regime. It is difficult to estimate the precise effects of the discretization and of the finite lattice spacing; by comparing the values in the second and third columns we see that the error decreases with the decrease of the lattice spacing, in agreement with expectations and implying that even finer lattices will yield higher-precision

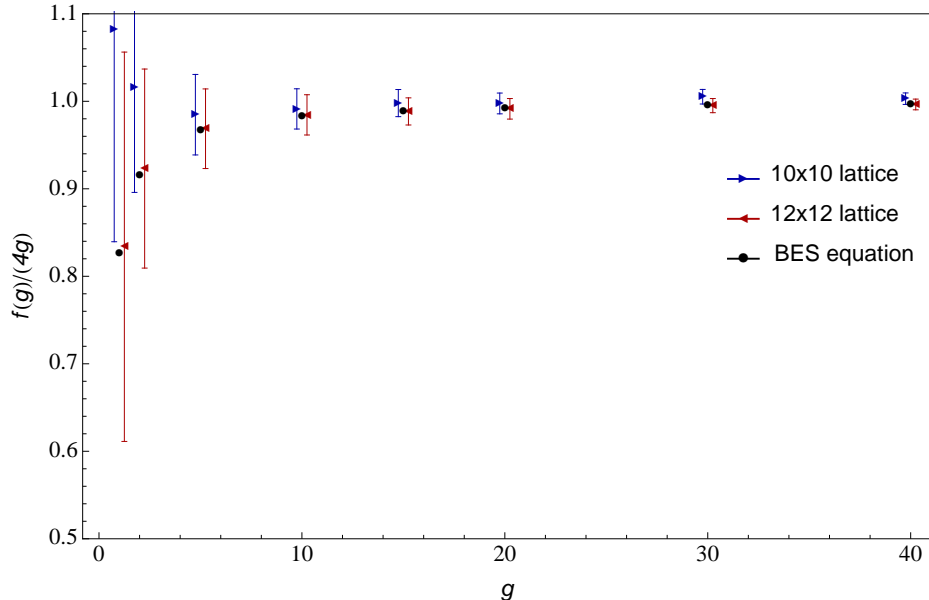


Figure 3: Plot of the rescaled universal scaling function from the 10×10 (blue right-triangles) and 12×12 (red left-triangles) and its values from the BES equation (black dots). The lattice values are artificially displaced by $\delta g = \pm 1/4$ for easy comparison. Clearly, the central values of the 12×12 lattice is a very good approximation of the integrability results.

results. We also ran these simulations for a smaller volume²² and found a substantial increase of the error estimate. This is consistent with an increase in the lower bound on the finite-volume uncertainty estimate (3.15).

In figure 3 we have plotted the three data sets rescaled by a factor of $(4g)$ such that at large values of g the graph asymptotes to one; to facilitate the comparison we also artificially shifted the plot along the horizontal axis by $\delta g = -1/4$ for the 10×10 lattice data and by $\delta g = +1/4$ for the 12×12 lattice data while keeping fixed the values obtained from the BES equation. We notice a very good agreement between the BES (black dots) and the central values of the 12×12 lattice results (red triangles) while still being in fair agreement within the error bars with the 10×10 lattice results (blue triangles).

Origin	a_0	a_1	a_2
10×10 lattice	4.031 ± 0.007	-0.667 ± 0.188	—
12×12 lattice	4.001 ± 0.002	-0.662 ± 0.041	-0.015 ± 0.066
perturbation theory	4.000 ± 0.000	-0.662 ± 0.001	-0.023 ± 0.001

Table 2: Coefficients of the fit of the lattice data with the expected form of the worldsheet perturbative expansion.

While the reported absolute errors for universal scaling functions are relatively large, we can try to make contact with worldsheet perturbation theory by fitting the lattice data in table 1

²²Increasing the lattice volume at fixed lattice spacing is computationally very expensive.

onto the known form of the worldsheet perturbation theory,

$$f(g) = a_0 g + a_1 + \frac{a_2}{g} + \dots \quad (3.16)$$

The resulting coefficients and their errors are listed in table 2. Not surprising, the quality of the fit degrades as one attempts to extract higher-order coefficients (*e.g.* an estimate for the two-loop coefficient cannot be extracted reliably from the 10×10 lattice). This is consistent with the observation that the first two terms in worldsheet perturbation theory provide a good approximation to the solution of the BES equation for $g > 1$. The fit may be slightly improved by assuming an expansion in $\sqrt{1 + 16g^2}$ rather than in g ; this accounts for the expected $g_* = 1/4$ radius of convergence of sYM perturbation theory. In particular, the central value of a_2 becomes very close to the results of perturbation theory at the expense of a slightly poorer fit for a_1 .

Origin \ g	10^{-1}	$(4\sqrt{\pi})^{-1}$	4^{-1}
12×12 lattice	0.014 ± 0.67	0.095 ± 0.69	0.581 ± 0.82
BES equation	0.077 ± 10^{-3}	0.150 ± 10^{-3}	0.427 ± 10^{-3}

Table 3: Values of the universal scaling function inside the radius of convergence of $\mathcal{N} = 4$ sYM theory.

We have also evaluated the universal scaling function for values of g at or below the expected radius of convergence of $\mathcal{N} = 4$ sYM perturbation theory, $g_* = 1/4$. The results are included in table 3. Since expected values for $f(g)$ are close to or below the expected lower bound of the error of the simulation on a lattice of volume $V_2 = \pi^2$, (3.15), the results cannot be statistically significant; we nevertheless note that, close to $g = g_*$, where the value of the cusp anomaly is larger than the error's lower bound, the central value is relatively close to the result of the BES equation. It should be possible – albeit nontrivial – to reduce the error bar on such data points. We also expect that further reducing the lattice spacing will lead to the central value moving closer to the BES prediction.

4 Summary and further comments

In this paper we computed the energy of the folded string in $\text{AdS}_5 \times \text{S}^5$ (and thus the universal scaling function) at finite values of the 't Hooft coupling using the Green-Schwarz string in $\text{AdS}_5 \times \text{S}^5$ by discretizing the worldsheet theory in the relevant background and computing numerically its partition function. Our results reproduce the predictions of the Asymptotic Bethe Ansatz within the accuracy of our simulation and thus strongly support the expectation that the Asymptotic Bethe Ansatz yields the long string spectrum, or the spectrum of long operators in the dual $\mathcal{N} = 4$ sYM theory for all values of the coupling. We have attempted to find the universal scaling function inside the radius of convergence of $\mathcal{N} = 4$ sYM theory; while our simulation is not sufficiently precise for this purpose, there is no conceptual obstacle.²³

²³These methods are however inappropriate for studying the regime $\lambda < 0$, whose existence is the reason for a finite radius of convergence for the planar theory.

Our calculation can in principle be extended to other long string states as well as to short string states that have a description as the small charge continuation of long string states. The computational complexity depends on the details of the state and is strongly correlated with the presence or absence of massless fermions. We have also discussed strategies for finding the spectrum of general string states that are not in this class from the two-point functions of certain worldsheet (vertex) operators. By computing the two-point function of worldsheet fluctuations in long string background it should be possible to find information on their spectra at finite values of the coupling.

The sources of errors in such calculations are well-understood; it turns out however that the single dominant source – related to the need to use a lattice of finite extent in both space-like and (Euclidean) time-like directions – is the most difficult to overcome. A volume increase at fixed lattice spacing requires an increase in the number of lattice sites which increases the duration of the calculation. A second – but not less important – consequence of the increase in the number of lattice sites is the rapid increase in the size of the fermion matrix (16^2 times faster than the increase in the number of lattice sites, due to the number of independent fermions); this in turn leads to either an increase in the time needed to find a solution to the systems (A.11) (necessary for the generation of field configurations) or a decrease in the accuracy of the solution.²⁴ It therefore appears that perhaps the most efficient improvement of our simulation is to employ a more efficient treatment of the fermion matrix. At the analytical level one may consider factorizing it into simpler (*e.g.* upper-triangular and lower-triangular) factors and exponentiating each factor separately. At the level of the numerical calculation one could attempt to use a Fourier-accelerated (R)HMC algorithm [56], which may reduce the thermalization time. One can also attempt to use a more efficient algorithm for solving the systems (A.11) (*e.g.* one that accepts a preconditioner – the numerical analog of the analytic factorization). Moreover, to alleviate the issues related to the size of the fermion matrix one could attempt to use a parallel GPU solver. A further possibility is to try to construct lattice actions that are much less sensitive to the lattice discretization than the one we used, perhaps along the lines of results in bosonic two-dimensional sigma models [57]. If such actions exist for the Green-Schwarz string they would allow use of larger lattice spacing while maintaining accuracy and thus would allow larger volume lattices.

The physically very interesting case of short string states provides a natural partial solution to the difficult consequences of a larger lattice volume. Indeed, the worldsheet of such strings is a cylinder and thus increasing the volume requires increasing only one of the two dimensions of the lattice. Consequently, the increase in the number of lattice sites occurs at a much slower rate allowing in principle for smaller finite-volume errors while simultaneously keeping the discretization and statistical errors under control. It would be very interesting analyze states on the first excited string level using the methods proposed in this paper.

²⁴Perhaps more dramatically, as the size of the matrix increases so does the memory needed to store it. One of the most expensive operations in the GPU calculations is data transfer; if the matrix is sufficiently large such that it cannot be fully stored on the GPU, most of the advantage of the GPU speedup is lost.

Acknowledgments

We would like to thank Joe Polchinski and Arkady Tseytlin for useful discussions. We would also like to thank Dima Volin for providing a numerical solution for the BES equation. This work is supported in part by the US Department of Energy under contract DE-SC0008745.

A Simulating the lattice: Algorithms

A.1 The Rational Hybrid Monte Carlo algorithm

In this appendix we review the structure of the Rational Hybrid Monte Carlo (RHMC) algorithm [33, 34, 35] which we used to simulate the Green-Schwarz string. It differs from the standard Hybrid Monte Carlo (HMC) algorithm [58] in the treatments of the fermion contribution for which it uses a rational approximation for the fractional power of the quadratic fermion matrix:

$$(M^\dagger M)^{-\frac{1}{4}} = \alpha_0 + \sum_{i=1}^P \frac{\alpha_i}{M^\dagger M + \beta_i} \quad (\text{A.1})$$

with real β_i . This approximation is obtained through the Remez algorithm [53, 35] implemented *e.g.* in `alg_remez` which is part of the library `RHMC-on-GPU`.

A.2 Monte Carlo methods

A method to evaluate high-dimensional integrals such as the path integrals necessary to evaluate expectation values of operators in quantum field theories with fields ϕ and Euclidean action $S_E[\phi]$

$$\langle \mathcal{O}(\phi) \rangle = \frac{1}{Z} \int D\phi \mathcal{O}(\phi) e^{-S_E[\phi]} \quad (\text{A.2})$$

is to randomly generate a sequence of field configurations with probability $P(\phi) = 1/Z \exp(-S_E[\phi])$ and then construct the “time” average

$$\overline{\mathcal{O}} = \frac{1}{T} \sum_{i=1}^T \mathcal{O}(\phi_i) . \quad (\text{A.3})$$

In the limit $T \rightarrow \infty$ the statistical expectation value $\langle \mathcal{O}(\phi) \rangle$ and the time-average $\overline{\mathcal{O}}$ are equal up to corrections $\mathcal{O}(T^{-1/2})$. A similar method is used to construct the partition function except that the normalization factor of the probability, $P(\phi) = \mathcal{N} \exp(-S_E[\phi])$, is chosen on physical grounds. A useful algorithm uses a Markov process which generates a new field configuration ϕ' from the old configuration ϕ with probability $P_M(\phi \rightarrow \phi')$ which samples the entire configuration space and satisfies

$$P_S(\phi)P_M(\phi \rightarrow \phi') = P_S(\phi')P_M(\phi' \rightarrow \phi) . \quad (\text{A.4})$$

These conditions guarantee convergence to a unique distribution P_S .

It is convenient to split the generation of the new field configuration in two steps: (1) one generates a new field configuration from the old one by some method and with some probability P_C and (2) one chooses between the newly generated configuration and the old one (to be called “new configuration” if chosen) with some probability P_A . Any information about the initial state will be lost after a sufficiently large number of steps. In this construction it is important that correlations between successive configurations be minimal; moreover, for the process to sample sufficiently quickly large parts of configuration space, it is useful to have a relatively large acceptance probability P_A , of the order of 50 – 90%.

A.3 The HMC algorithm

An elegant method which realizes these ideas is the Hybrid Monte Carlo (HMC) algorithm proposed in ref. [58]; a deterministic molecular dynamics evolution is used to generate new field configurations and a stochastic Metropolis acceptance test is used to select the configurations which are retained; see *e.g.* [59] for a thorough discussion of this algorithm and its variations.

Denoting by the index ϕ and ζ the bosonic fields and the pseudo-fermions (cf. eq. (2.3)), ref. [58] postulates the Hamiltonian

$$H_\tau = \frac{1}{2}\pi_\phi^2 + \bar{\pi}_\zeta\pi_\zeta + S_\phi + S_\zeta , \quad (\text{A.5})$$

which describes the evolution along some fictitious direction τ . All fields are assumed to depend on this fictitious coordinate. The new fields π_ϕ and π_ζ are interpreted as momenta conjugate to bosons and pseudo-fermions. The partition function with this Hamiltonian is the partition function with the action $S_b + S_\zeta$ up to a normalization factor from integrating out π_ϕ and π_ζ . This factor may be found by computing the partition function with $S_\phi + S_\zeta = 0$

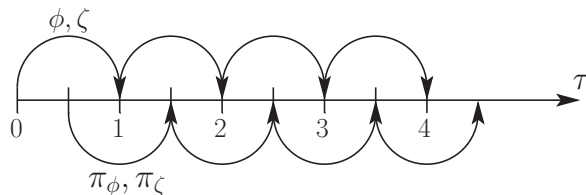


Figure 4: Sketch of the Leapfrog method: where values of fields and their conjugate momenta “leap” over each other.

Given some initial field configuration (ϕ, ζ) and some randomly generated momenta π_ϕ and π_ζ a new field configuration is constructed deterministically by solving Hamilton’s equations of motion for H_τ :

$$\partial_\tau \pi_\phi = -\frac{\partial H_\tau}{\partial \phi} \equiv F_\phi \quad \partial_\tau \pi_\zeta = -\frac{\partial H_\tau}{\partial \zeta} \equiv F_\zeta \quad (\text{A.6})$$

$$\partial_\tau \phi = \frac{\partial H}{\partial \pi_\phi} = \pi_\phi \quad \partial_\tau \zeta = \frac{\partial H}{\partial \pi_\zeta} = \bar{\pi}_\zeta , \quad (\text{A.7})$$

where F_ϕ and F_ζ are bosonic and fermionic “forces”. These equations are integrated with an energy-conserving symplectic (*i.e.* phase space-area preserving) integrator that uses the standard leapfrog scheme: we update the values of fields and their conjugate momenta at staggered time steps, such that one is leaping over the other, see figure 4. For the bosons ϕ the evolution over $\delta\tau$ is given by

$$\pi_{\phi,\tau+\delta\tau/2} = \pi_{\phi,\tau} + F_{\phi,\text{initial}} \frac{\delta\tau}{2} \quad , \quad \phi_{\tau+\delta\tau} = \phi_\tau + \pi_{\tau+\delta\tau/2} \delta\tau \quad (\text{A.8})$$

$$\pi_{\phi;\tau+\delta\tau} = \pi_{\phi;\tau+\delta\tau/2} + F_{\phi;\text{updated}} \frac{\delta\tau}{2} \quad . \quad (\text{A.9})$$

The evolution of ζ and π_ζ is similar. This integration method introduces only an $\mathcal{O}(\delta\tau^2)$ error.²⁵

To eliminate this artificial error the field configuration obtained after some number n_T of time steps – known as an HMC trajectory – undergoes a Metropolis acceptance step [58]: a number $n_M \in [0, 1]$ is randomly generated and the final configuration is accepted if $n_M < e^{-\delta H_\tau}$ where δH_τ is the change in the value of the Hamiltonian (A.5) between the initial and final field configuration of that trajectory. If $e^{-\delta H_\tau} < n_M$ then the initial field configuration is accepted as the new field configuration contributing to (A.3). At the beginning of each HMC trajectory – *i.e.* after each Metropolis test – momenta are refreshed based on a Gaussian distribution (centered at zero and with unit standard deviation), which will keep the simulation ergodic. Since in the limit $\delta\tau \rightarrow 0$ the integrator preserves the energy, the only reason $e^{-\delta H}$ might not equal unity is the presence of some error due to the finite time-step $\delta\tau$. The inclusion of the Metropolis acceptance step renders the HMC algorithm exact, with results independent of step size [58] (reversibility of the dynamics is important for proving this).

A.4 The fermion contribution to bosonic RHMC forces

Due to the rational approximation (A.1) of $(M_{\text{string}}^\dagger M_{\text{string}})^{-\frac{1}{4}}$, the fermionic contribution to the bosonic forces takes a relatively simple form, which suggests an efficient way to evaluate it. Denoting as before a generic boson by ϕ and the pseudo-fermions by ζ , the pseudo-fermion

²⁵To see this [60] one compares the infinitesimal evolution with $H_\tau = T(\pi_\phi, \pi_\zeta) + S(\phi, \zeta)$ with the step-wise evolution operator (A.9),

$$e^{-(S+T)\delta\tau} \quad \text{vs.} \quad e^{-\frac{1}{2}\delta\tau S} e^{-\delta\tau T} e^{-\frac{1}{2}\delta\tau S} \quad .$$

Using the Baker-Campbell-Hausdorff relation

$$\begin{aligned} e^X e^Y &= e^{C(X,Y)} \quad C(X,Y) = C_1(X,Y) + C_2(X,Y) + C_3(X,Y) + \dots \\ C_1 &= X + Y \quad C_2 = \frac{1}{2}[X,Y] \quad C_3 = \frac{1}{12}([X,Y], Y) - \frac{1}{12}([X,Y], X) \end{aligned}$$

and the fact that the action of S and T is given by the Poisson brackets of momenta and fields, the two evolution operators can be easily related:

$$e^{-\frac{1}{2}\delta\tau S} e^{-\delta\tau T} e^{-\frac{1}{2}\delta\tau S} \simeq \exp\{-\delta\tau(S+T) - \delta\tau^3([S,T], S) + \frac{1}{2}\delta\tau^3([S,T], T) + \mathcal{O}(\delta\tau^5)\} \quad .$$

The antisymmetry of the Poisson bracket leads to the cancellation of the contribution of the commutator C_2 in the Baker-Campbell-Hausdorff formula. Thus, the two evolution operators differ by terms suppressed by a factor of $\delta\tau^2$.

contribution to the bosonic forces F_ϕ^ζ is:

$$\begin{aligned}
F_\phi^\zeta &= -\frac{\partial S_\zeta}{\partial \phi} = \sum_{i=1}^P \alpha_i \left(\frac{1}{M^\dagger M + \beta_i} \zeta \right)^\dagger \frac{\partial}{\partial \phi} (M^\dagger M) \left(\frac{1}{M^\dagger M + \beta_i} \zeta \right) \\
&= \sum_{i=1}^P \left[\alpha_i \left(M \frac{1}{M^\dagger M + \beta_i} \zeta \right)^\dagger \frac{\partial M}{\partial \phi} \left(\frac{1}{M^\dagger M + \beta_i} \zeta \right) \right. \\
&\quad \left. + \alpha_i \left(\frac{1}{M^\dagger M + \beta_i} \zeta \right)^\dagger \frac{\partial M^\dagger}{\partial \phi} \left(M \frac{1}{M^\dagger M + \beta_i} \zeta \right) \right] \\
&= \sum_{i=1}^P \alpha_i \left((M s_i)^\dagger \frac{\partial M}{\partial \phi} s_i + s_i^\dagger \frac{\partial M^\dagger}{\partial \phi} M s_i \right) , \tag{A.10}
\end{aligned}$$

where $s_i = 1/(M^\dagger M + \beta_i)\zeta$ are interpreted as the solutions to the matrix equation

$$(M^\dagger M + \beta_i) s_i = \zeta \quad , \quad i = 1, \dots, P . \tag{A.11}$$

In the discretized theory ζ stands for the vector of values of the field ζ at all lattice sites, $M^\dagger M$ is a matrix of size (nr. of fermion components \times nr. of lattice sites)². For example, for the cusp anomaly calculation in section 3 on the 12×12 lattice, $M^\dagger M$ has size $(16 * 12^2) \times (16 * 12^2)$ and ζ stands for a $(16 * 12^2)$ -component vector comprising all the components (16) pseudo-fermions at all lattice sites (12^2).

The systems (A.11) are solved using a multi-mass conjugate gradient solver – in particular `gc_m` routine which is part of the CUSP library [61] – the which allows for the solution of all P systems in a single solve. As long as all the shifts β_i are positive one can solve for the entire family of solutions at the cost of solving for a single unshifted system: one solves for the shifted system with slowest convergence²⁶ and then the other shifted solutions can be found by an additional multiplication step [62]. The standard conjugate gradient solver is described in [63].

With the same notation the fermionic forces are:

$$F_\zeta = -\frac{\partial S_\zeta}{\partial \zeta} = -\alpha_0 \frac{\partial}{\partial \zeta} (\zeta^\dagger \zeta) - \sum_{i=1}^P \frac{\partial}{\partial \zeta} \left(\zeta^\dagger \frac{\alpha_i}{M^\dagger M + \beta_i} \zeta \right) = -\alpha_0 \zeta^\dagger - \sum_{i=1}^P \alpha_i s_i^\dagger \tag{A.12}$$

and are determined by the solution to the same system (A.11). Even though the fermionic matrix, $M^\dagger M$, is not guaranteed to be symmetric, its hermiticity guarantees that the multi-mass conjugate-gradient method will yield a solution to (A.11) [64, 63].

A.5 A summary of sources of errors

The RHMC algorithm is considered to be an exact algorithm to machine precision [58]. Nevertheless, errors are introduced through the approximations made in the construction of the simulation; they have both a statistical and a systematic origin. We summarize here the ones relevant for the Green-Schwarz string in $\text{AdS}_5 \times \text{S}^5$ space:

²⁶ $\beta_i=0$ is the slowest-converging system.

- Statistical error – arises because the path integral (with or without additional operator insertions) is approximated in terms of a finite number of field configurations. In our calculations we employed $\mathcal{O}(500)$ independent configurations. Statistical errors may be reduced by increasing the number of field configurations.
- Discretization errors – arise because of the finite lattice spacing and in the extrapolation to the continuum limit. In two dimensions the approach to the continuum limit is accompanied by a quadratic increase in the number of lattice sites which in turn leads to an increase in the computational cost at a higher rate. These errors may be reduced by employing higher-point approximations for field derivatives.
- Other approximation errors – arise because of the Remez algorithm used to construct a rational approximation of the inverse fractional power as well as because of the numerical errors of the multi-mass conjugate-gradient solver. The former may be reduced by using more terms in eq. A.1. The latter may potentially be reduced by improving the treatment of the fermion matrix, such as using a preconditioner and other algorithms for solving the linear systems (A.11).
- Finite volume errors – all simulations are carried out on lattices of finite extent. Since the Compton wave length of a massive particle is proportional to its inverse mass, finite volume effects are larger for particles of smaller masses. In the context of our calculations we have estimated these errors in sec. 3.1.

B 9-point stencil

We want to construct a discrete approximation to the derivative of some function $f(x)$ such that the error is of the order $\mathcal{O}(a^8)$ where a is the lattice spacing. This requires a nine-point stencil using $f(x \pm a), f(x \pm 2a), f(x \pm 3a), f(x \pm 4a)$. We expand then in Taylor series around $a = 0$ to $\mathcal{O}(a^8)$ and then solve the resulting system for $\partial_x f(x)$:

$$f(x \pm a) = f(x) \pm a f^{(1)}(x) + \frac{1}{2} a^2 f^{(2)}(x) \pm \frac{1}{3!} a^3 f^{(3)}(x) + \frac{1}{4!} a^4 f^{(4)}(x) \quad (\text{B.1})$$

$$\pm \frac{1}{5!} a^5 f^{(5)}(x) + \frac{1}{6!} a^6 f^{(6)}(x) \pm \frac{1}{7!} a^7 f^{(7)}(x) + \mathcal{O}(a^8) \quad (\text{B.2})$$

$$f(x \pm 2a) = f(x) \pm 2a f^{(1)}(x) + 2a^2 f^{(2)}(x) \pm \frac{4}{3} a^3 f^{(3)}(x) + \frac{2}{3} a^4 f^{(4)}(x) \quad (\text{B.3})$$

$$\pm \frac{2^5}{5!} a^5 f^{(5)}(x) + \frac{2^6}{6!} a^6 f^{(6)}(x) \pm \frac{2^7}{7!} a^7 f^{(7)}(x) + \mathcal{O}(a^8) \quad (\text{B.4})$$

$$f(x \pm 3a) = f(x) \pm 3a f^{(1)}(x) + \frac{9}{2} a^2 f^{(2)}(x) \pm \frac{9}{2} a^3 f^{(3)}(x) + \frac{27}{8} a^4 f^{(4)}(x) \quad (\text{B.5})$$

$$\pm \frac{3^5}{5!} a^5 f^{(5)}(x) + \frac{3^6}{6!} a^6 f^{(6)}(x) \pm \frac{3^7}{7!} a^7 f^{(7)}(x) + \mathcal{O}(a^8) \quad (\text{B.6})$$

$$f(x \pm 4a) = f(x) \pm 4a f^{(1)}(x) + 8a^2 f^{(2)}(x) \pm \frac{32}{3} a^3 f^{(3)}(x) + \frac{32}{3} a^4 f^{(4)}(x) \quad (\text{B.7})$$

$$\pm \frac{4^5}{5!} a^5 f^{(5)}(x) + \frac{4^6}{6!} a^6 f^{(6)}(x) \pm \frac{4^7}{7!} a^7 f^{(7)}(x) + \mathcal{O}(a^8) \quad (\text{B.8})$$

Requiring that

$$\begin{aligned} \alpha a \partial_x f(x) + \mathcal{O}(a^9) &= e(f(x+a) - f(x-a)) - b(f(x+2a) - f(x-2a)) \\ &\quad - c(f(x+3a) - f(x-3a)) - d(f(x+4a) - f(x-4a)) \end{aligned} \quad (\text{B.9})$$

constrains the coefficients on the right-hand side to be a solution of the system

$$\begin{aligned} e - 8b - 27c - 64d &= 0 \\ e - 32b - 243c - 1024d &= 0 \\ e - 128b - 2187c - 16384d &= 0 \end{aligned} \quad (\text{B.10})$$

The solution $e = 224, b = 56, c = -\frac{32}{3}, d = 1$ leads to $\alpha = 280$ and to the nine-point stencil quoted in eq. (3.10).

B.1 ρ matrices

We include here the explicit form of the matrices ρ^M entering the AdS light-cone gauge action. They are off-diagonal blocks of the six-dimensional Dirac matrices in chiral representation:

$$\rho_{ij}^M = -\rho_{ji}^M, \quad (\rho^M)^{il} \rho_{lj}^N + (\rho^N)^{il} \rho_{lj}^M = 2\delta^{MN} \delta_j^i, \quad (\rho^M)^{ij} \equiv -(\rho_{ij}^M)^* \quad (\text{B.11})$$

$$\rho^{MNi}{}_j = \frac{1}{2} [(\rho^M)^{il} \rho_{lj}^N - (\rho^N)^{il} \rho_{lj}^M]. \quad (\text{B.12})$$

One can choose the following explicit representation for the ρ_{ij}^M matrices

$$\begin{aligned} \rho_{ij}^1 &= \begin{pmatrix} 0 & 1 & 0 & 0 \\ -1 & 0 & 0 & 0 \\ 0 & 0 & 0 & 1 \\ 0 & 0 & -1 & 0 \end{pmatrix}, & \rho_{ij}^2 &= \begin{pmatrix} 0 & i & 0 & 0 \\ -i & 0 & 0 & 0 \\ 0 & 0 & 0 & -i \\ 0 & 0 & i & 0 \end{pmatrix}, & \rho_{ij}^3 &= \begin{pmatrix} 0 & 0 & 0 & 1 \\ 0 & 0 & 1 & 0 \\ 0 & -1 & 0 & 0 \\ -1 & 0 & 0 & 0 \end{pmatrix}, \\ \rho_{ij}^4 &= \begin{pmatrix} 0 & 0 & 0 & -i \\ 0 & 0 & i & 0 \\ 0 & -i & 0 & 0 \\ i & 0 & 0 & 0 \end{pmatrix}, & \rho_{ij}^5 &= \begin{pmatrix} 0 & 0 & i & 0 \\ 0 & 0 & 0 & i \\ -i & 0 & 0 & 0 \\ 0 & -i & 0 & 0 \end{pmatrix}, & \rho_{ij}^6 &= \begin{pmatrix} 0 & 0 & 1 & 0 \\ 0 & 0 & 0 & -1 \\ -1 & 0 & 0 & 0 \\ 0 & 1 & 0 & 0 \end{pmatrix}, \end{aligned}$$

C Fermions

After the introduction of the auxiliary fields ϕ and ϕ_M the fermion Lagrangian is quadratic:

$$L_{\text{fermions}} = \psi^T M \psi. \quad (\text{C.1})$$

For the AdS light-cone gauge action $\psi \equiv (\tilde{\theta}^i, \tilde{\theta}_i, \tilde{\eta}^i, \tilde{\eta}_i)$ and in the background of the null cusp solution M is given by:

$$\begin{aligned} &M_{\text{cusp}} \\ &= \begin{pmatrix} 0 & i\partial_t \mathbf{1}_4 & -i(\partial_s + \frac{1}{2})\rho^M \frac{\tilde{z}^M}{\tilde{z}^3} & 0 \\ i\partial_t \mathbf{1}_4 & 0 & 0 & -i(\partial_s + \frac{1}{2})\rho_M^\dagger \frac{\tilde{z}^M}{\tilde{z}^3} \\ i\rho^M \frac{\tilde{z}^M}{\tilde{z}^3} (\partial_s - \frac{1}{2}) & 0 & -\rho^M \frac{\tilde{z}^M}{\tilde{z}^4} (\partial_s \tilde{x} - \frac{\tilde{x}}{2} - \tilde{x} \partial_s) & i\partial_t \mathbf{1}_4 + A^\dagger \\ 0 & i\rho_M^\dagger \frac{\tilde{z}^M}{\tilde{z}^3} (\partial_s - \frac{1}{2}) & i\partial_t \mathbf{1}_4 + A & -\rho_M^\dagger \frac{\tilde{z}^M}{\tilde{z}^4} (\partial_s \tilde{x}^* - \frac{\tilde{x}^*}{2} - \tilde{x}^* \partial_s) \end{pmatrix} \end{aligned} \quad (\text{C.2})$$

with A given by

$$A = \frac{1}{\tilde{z}^4} \tilde{\phi}^M \rho^{MN} \tilde{z}^N + \frac{1}{\tilde{z}^2} \tilde{\phi} + \frac{i}{\tilde{z}^2} \tilde{z}^N \rho^{MN} (\partial_t \tilde{z}^M) . \quad (\text{C.3})$$

References

- [1] I. Bena, J. Polchinski and R. Roiban, “*Hidden symmetries of the AdS(5) x S**5 superstring*”, Phys.Rev. D69, 046002 (2004), hep-th/0305116.
- [2] B. C. Vallilo, “*Flat currents in the classical AdS(5) x S**5 pure spinor superstring*”, JHEP 0403, 037 (2004), hep-th/0307018.
- [3] N. Berkovits, “*Quantum consistency of the superstring in AdS(5) x S**5 background*”, JHEP 0503, 041 (2005), hep-th/0411170.
- [4] N. Beisert, B. Eden and M. Staudacher, “*Transcendentality and Crossing*”, J.Stat.Mech. 0701, P01021 (2007), hep-th/0610251.
- [5] G. Arutyunov and S. Frolov, “*Thermodynamic Bethe Ansatz for the AdS(5) x S(5) Mirror Model*”, JHEP 0905, 068 (2009), 0903.0141.
- [6] N. Gromov, V. Kazakov and P. Vieira, “*Exact Spectrum of Anomalous Dimensions of Planar N=4 Supersymmetric Yang-Mills Theory*”, Phys.Rev.Lett. 103, 131601 (2009), 0901.3753.
- [7] D. M. Hofman and J. M. Maldacena, “*Giant Magnons*”, J.Phys. A39, 13095 (2006), hep-th/0604135.
- [8] T. Klose, T. McLoughlin, J. Minahan and K. Zarembo, “*World-sheet scattering in AdS(5) x S**5 at two loops*”, JHEP 0708, 051 (2007), 0704.3891.
- [9] D. Berenstein and D. Trancanelli, “*S-duality and the giant magnon dispersion relation*”, 0904.0444.
- [10] D. J. Gross, A. Mikhailov and R. Roiban, “*Operators with large R charge in N=4 Yang-Mills theory*”, Annals Phys. 301, 31 (2002), hep-th/0205066.
- [11] A. Santambrogio and D. Zanon, “*Exact anomalous dimensions of N=4 Yang-Mills operators with large R charge*”, Phys.Lett. B545, 425 (2002), hep-th/0206079.
- [12] N. Beisert, “*The SU(2|2) dynamic S-matrix*”, Adv.Theor.Math.Phys. 12, 945 (2008), hep-th/0511082.
- [13] Z. Bern, M. Czakon, L. J. Dixon, D. A. Kosower and V. A. Smirnov, “*The Four-Loop Planar Amplitude and Cusp Anomalous Dimension in Maximally Supersymmetric Yang-Mills Theory*”, Phys.Rev. D75, 085010 (2007), hep-th/0610248.
- [14] F. Cachazo, M. Spradlin and A. Volovich, “*Four-loop cusp anomalous dimension from obstructions*”, Phys.Rev. D75, 105011 (2007), hep-th/0612309.
- [15] S. Giombi, R. Ricci, R. Roiban, A. Tseytlin and C. Vergu, “*Quantum AdS(5) x S5 superstring in the AdS light-cone gauge*”, JHEP 1003, 003 (2010), 0912.5105.
- [16] S. Giombi, R. Ricci, R. Roiban, A. Tseytlin and C. Vergu, “*Generalized scaling function from light-cone gauge AdS5 x S5 superstring*”, JHEP 1006, 060 (2010), 1002.0018.
- [17] S. Leurent, D. Serban and D. Volin, “*Six-loop Konishi anomalous dimension from the Y-system*”, Phys.Rev.Lett. 109, 241601 (2012), 1209.0749.

- [18] N. Gromov, V. Kazakov and P. Vieira, “*Exact Spectrum of Planar $\mathcal{N} = 4$ Supersymmetric Yang-Mills Theory: Konishi Dimension at Any Coupling*”, Phys.Rev.Lett. 104, 211601 (2010), 0906.4240.
- [19] B. Eden, P. Heslop, G. P. Korchemsky, V. A. Smirnov and E. Sokatchev, “*Five-loop Konishi in $N=4$ SYM*”, Nucl.Phys. B862, 123 (2012), 1202.5733.
- [20] R. Roiban and A. Tseytlin, “*Semiclassical string computation of strong-coupling corrections to dimensions of operators in Konishi multiplet*”, Nucl.Phys. B848, 251 (2011), 1102.1209.
- [21] N. Gromov, D. Serban, I. Shenderovich and D. Volin, “*Quantum folded string and integrability: From finite size effects to Konishi dimension*”, JHEP 1108, 046 (2011), 1102.1040.
- [22] M. Beccaria, S. Giombi, G. Macorini, R. Roiban and A. Tseytlin, “*‘Short’ spinning strings and structure of quantum $AdS_5 \times S^5$ spectrum*”, Phys.Rev. D86, 066006 (2012), 1203.5710.
- [23] B. Basso, G. Korchemsky and J. Kotanski, “*Cusp anomalous dimension in maximally supersymmetric Yang-Mills theory at strong coupling*”, Phys.Rev.Lett. 100, 091601 (2008), 0708.3933.
- [24] S. Catterall and G. van Anders, “*First Results from Lattice Simulation of the PWMM*”, JHEP 1009, 088 (2010), 1003.4952.
- [25] S. Catterall and T. Wiseman, “*Gauge-gravity duality – Super Yang Mills Quantum Mechanics*”, PoS LAT2007, 051 (2007), 0709.3497.
- [26] S. Catterall and S. Ghadab, “*Twisted supersymmetric sigma model on the lattice*”, JHEP 0610, 063 (2006), hep-lat/0607010.
- [27] W. Siegel, “*Randomizing the superstring*”, Phys.Rev. D50, 2799 (1994), hep-th/9403144.
- [28] M. Hatsuda and W. Siegel, “*A New holographic limit of $AdS(5) \times S^{**5}$* ”, Phys.Rev. D67, 066005 (2003), hep-th/0211184.
- [29] H. Nastase and W. Siegel, “*A New AdS / CFT correspondence*”, JHEP 0010, 040 (2000), hep-th/0010106.
- [30] K. G. Wilson, “*Confinement of Quarks*”, Phys.Rev. D10, 2445 (1974).
- [31] S. Catterall, “*Notes on (twisted) lattice supersymmetry*”, hep-lat/0510054.
- [32] S. Catterall, D. Kaplan and M. Unsal, “*Exact lattice supersymmetry*”, Phys.Rept. 484, 71 (2009), 0903.4881.
- [33] A. Kennedy, I. Horvath and S. Sint, “*A New exact method for dynamical fermion computations with nonlocal actions*”, Nucl.Phys.Proc.Suppl. 73, 834 (1999), hep-lat/9809092.
- [34] M. Clark and A. Kennedy, “*The RHMC algorithm for two flavors of dynamical staggered fermions*”, Nucl.Phys.Proc.Suppl. 129, 850 (2004), hep-lat/0309084.
- [35] M. Clark, “*The Rational Hybrid Monte Carlo Algorithm*”, PoS LAT2006, 004 (2006), hep-lat/0610048.
- [36] J. Giedt, “*The Fermion determinant in $(4,4)$ 2-d lattice superYang-Mills*”, Nucl.Phys. B674, 259 (2003), hep-lat/0307024.
- [37] U. J. Wiese, “*An introduction to lattice field theory*”.
- [38] R. Kallosh and J. Rahmfeld, “*The GS string action on $AdS(5) \times S^{**5}$* ”, Phys.Lett. B443, 143 (1998), hep-th/9808038.

- [39] R. Kallosh and A. A. Tseytlin, “*Simplifying superstring action on $AdS(5) \times S^{**5}$* ”, JHEP 9810, 016 (1998), hep-th/9808088.
- [40] R. Roiban and W. Siegel, “*Superstrings on $AdS(5) \times S^{**5}$ supertwistor space*”, JHEP 0011, 024 (2000), hep-th/0010104.
- [41] R. Metsaev, C. B. Thorn and A. A. Tseytlin, “*Light cone superstring in AdS space-time*”, Nucl.Phys. B596, 151 (2001), hep-th/0009171.
- [42] G. Arutyunov and S. Frolov, “*Foundations of the $AdS_5 \times S^5$ Superstring. Part I*”, J.Phys. A42, 254003 (2009), 0901.4937.
- [43] T. Banks and A. Casher, “*Chiral Symmetry Breaking in Confining Theories*”, Nucl.Phys. B169, 103 (1980).
- [44] N. Beisert, C. Ahn, L. F. Alday, Z. Bajnok, J. M. Drummond et al., “*Review of AdS/CFT Integrability: An Overview*”, Lett.Math.Phys. 99, 3 (2012), 1012.3982.
- [45] A. Tirziu and A. A. Tseytlin, “*Quantum corrections to energy of short spinning string in $AdS(5)$* ”, Phys.Rev. D78, 066002 (2008), 0806.4758.
- [46] R. Roiban and A. A. Tseytlin, “*Quantum strings in $AdS(5) \times S^{**5}$: Strong-coupling corrections to dimension of Konishi operator*”, JHEP 0911, 013 (2009), 0906.4294.
- [47] A. M. Polyakov, “*Gauge fields and space-time*”, Int.J.Mod.Phys. A17S1, 119 (2002), hep-th/0110196.
- [48] A. A. Tseytlin, “*On semiclassical approximation and spinning string vertex operators in $AdS(5) \times S^{**5}$* ”, Nucl.Phys. B664, 247 (2003), hep-th/0304139.
- [49] R. Roiban and A. Tseytlin, “*On semiclassical computation of 3-point functions of closed string vertex operators in $AdS_5 \times S^5$* ”, Phys.Rev. D82, 106011 (2010), 1008.4921.
- [50] S. Frolov and A. A. Tseytlin, “*Semiclassical quantization of rotating superstring in $AdS(5) \times S^{**5}$* ”, JHEP 0206, 007 (2002), hep-th/0204226.
- [51] S. Frolov, A. Tirziu and A. A. Tseytlin, “*Logarithmic corrections to higher twist scaling at strong coupling from AdS/CFT* ”, Nucl.Phys. B766, 232 (2007), hep-th/0611269.
- [52] R. Roiban and A. A. Tseytlin, “*Spinning superstrings at two loops: Strong-coupling corrections to dimensions of large-twist SYM operators*”, Phys.Rev. D77, 066006 (2008), 0712.2479.
- [53] E. Y. Remez, “*Sur le calcul effectif des polynmes d’approximation de Tschebyscheff*”, C. R. Acad. Sci., Paris 199, 337340 (1934).
- [54] S. Giombi, R. Ricci, R. Roiban and A. Tseytlin, “*Two-loop $AdS_5 \times S^5$ superstring: testing asymptotic Bethe ansatz and finite size corrections*”, J.Phys. A44, 045402 (2011), 1010.4594.
- [55] J. Simone, “*Data analysis using the Gnu R system for statistical computation*”, PoS LATTICE2011, 048 (2011).
- [56] S. Catterall and S. Karamov, “*Testing a Fourier accelerated hybrid Monte Carlo algorithm*”, Phys.Lett. B528, 301 (2002), hep-lat/0112025.
- [57] J. Balog, F. Niedermayer, M. Pepe, P. Weisz and U.-J. Wiese, “*Drastic Reduction of Cutoff Effects in 2-d Lattice $O(N)$ Models*”, JHEP 1211, 140 (2012), 1208.6232.
- [58] S. Duane, A. D. Kennedy, B. J. Pendleton and D. Roweth, Phys. Lett. B195:, 216 (1987).

- [59] R. M. Neal, “*MCMC using Hamiltonian dynamics*”, 1206.1901, in: “*Handbook of Markov Chain Monte Carlo*”, ed.: S. Brooks, A. Gelman, G. L. Jones and X.-L. Meng, Chapman & Hall / CRC Press (2010), 113-162p.
- [60] J. Sexton and D. Weingarten, “*Hamiltonian evolution for the hybrid Monte Carlo algorithm*”, Nucl.Phys. B380, 665 (1992).
- [61] N. Bell and M. Garland, “*Cusp: Generic Parallel Algorithms for Sparse Matrix and Graph Computations*”, Version 0.3.0, <http://cusp-library.googlecode.com>.
- [62] B. Jegerlehner, “*Krylov space solvers for shifted linear systems*”, hep-lat/9612014.
- [63] E. S. M. R. Hestenes, J. Res. Nat. Bureau of Standards 49, 409 ((1952)).
- [64] T. Ten, J. E. Drut and T. A. Lahde, “*Preconditioning the non-relativistic many-fermion problem*”, 1008.3647.